Desalination and Water Treatment
www.deswater.com
doi: 10.5004/dwt.2019.24243

158 (2019) 343–352
August

Optimization of methylene blue biosorption and mass transfer resistance on *Gardenia carinata* activated carbon

Ezerie Henry Ezechi*, Khalida Muda

School of Civil Engineering, Universiti Teknologi Malaysia 81310, Johor Bahru, Malaysia, Tel. +601139654522; email: honhenry2k5@gmail.com (E.H. Ezechi); Tel. +07-5531522; email: khalida@utm.my (K .Muda)

Received 27 November 2018; Accepted 8 April 2019

ABSTRACT

This study evaluated Methylene blue (MB) adsorption from dye effluent using a new activated carbon derived from *Gardenia carinata*. The derived *Gardenia carinata* activated carbon (GCAC) has a large surface area of 1,187.33 m^2/g. Experiments were designed with the central composite design model of the response surface methodology. The interaction between independent variables (adsorbent mass, pH and initial MB concentration) was evaluated at pre-determined contact time of 30 min. Results show that MB adsorption decreased with increasing pH from 4 to 10 but increased with increasing adsorbent mass and initial concentration. MB adsorption exceeded 89% at optimum conditions. Kinetic examination indicated no mass transfer resistance with increasing MB concentration. The driving force (*B*) of MB transport increased from 3.621 to 4.906 mg/g with increasing MB concentration. Furthermore, the adsorbate/adsorbent attraction increased from 10.570 to 17.064 g/h/mg with increasing MB concentration. This study demonstrates that activated carbon derived from abundant waste materials such as *Gardenia carinata* can be useful in many significant ways.

Keywords: Adsorption; Adsorbent; *Gardenia*; Methylene blue; Response surface methodology; Central composite design; Mass transfer

1. Introduction

Dyes and pigments have wide industrial applications in paper, leather, textile, printing and cosmetic industries. Consumption of dyes and pigments in these industries is estimated at about 0.7–0.9 million ton/year [1,2]. A significant portion (about 10%) of these dyes are lost during coloration in the textile industries while 2% are directly discharged in aqueous effluent [3]. Some of these dyes are harmful, hazardous, recalcitrant and unsafe [4]. Particularly, azo dyes possess genotoxic and carcinogenic properties and their effluent degradation products are generated in excess of 4,500,000 ton annually. Most disperse azo dyes in discharged effluents are found chemically stable or unchanged due to their hydrophobic nature [5]. For instance, Carneiro et al. [5] found that a river in Brazil contains different levels of disperse dyes due to effluent discharge. Such dye-contaminated water can cause severe lesions of the colon in rats at exposure of 1%–10% [6]. Therefore, indiscriminate discharge of disperse dye polluted effluent into water bodies can be deleterious to both terrestrial and aquatic ecosystem [7]. It is, therefore, urgent to reduce the presence of dye in effluent.

Adsorption process using activated carbon is a technique known and used for the isolation of various wastewater pollutants. Activated carbons (ACs) are characterized with high surface area and large porosity. These characteristics have increased its application in adsorption processes [8]. Primary ACs were mainly of commercial types. Due to the cost of industrial ACs, attention was directed to obtaining AC from solid and lignocellulosic waste from agriculture. Agricultural waste such as sugar cane bagasse [9,10], peanut

* Corresponding author.

husk [11], peanut hull [12], bamboo [13], coconut shell [14], empty fruit bunch [15] and rice husk [16–18] are suitable AC resources. The capacity of several un-modified adsorbents such as gulmohar plant leaf powder [19], ageratum conyzoide leaf powder [20,21] and neem leaf powder [22] has also been investigated.

In conventional adsorption technique, one parameter is varied while other parameters are set constant. This technique is costly, non-optimizable and takes a longer time [23]. In contrast, response surface methodology (RSM) lowers the cost of experiments by reducing experimental runs. RSM uses experimental data to explain the interactive effect of process variables. It can build, analyze and define the behavior of a model from results calculated within different regions in the design space [24]. It optimizes the experimental conditions by identifying the optimum region from the design space [25–27]. RSM has emerged as a reliable tool for mathematical modeling and has been applied in a wide range of studies.

The basic adsorption mechanisms involve the transport of solutes over a liquid film covering a solid porous material, transfer of solutes from the pores of the internal structure of the solid materials into the active sites or intraparticle diffusion and transfer of solutes onto the internal surface pores of the solid material [28,29]. These mass transfer mechanisms can be influenced by various experimental factors including stirring speed, adsorbent size [29], adsorbent porosity, adsorbate solubility [30] and initial solute concentration. Therefore, it is important to examine the mass transfer resistance during adsorption process.

Gardenia is a flowering plant belonging to the Rubiaceae family. The plant is abundantly native to tropical and subtropical regions. *Gardenia* has important medicinal application in the treatment of various diseases [31]. *Gardenia carinata* is an abundant specie of the *Gardenia* genus that produces small to medium size seeds. Its seeds are shelly, medium (1–5 cm length and width) and highly carbonaceous. The seeds frequently fall off the trees and loiter the environment. This scenario raises legitimate environmental concerns over solid waste management in light of aging landfills [32]. Therefore, the conversion of *Gardenia carinata* shell into a biosorbent has two unique benefits. First, the production of a low cost value added product useful for wastewater treatment and second, reduction of the environmental pollution caused by the decaying *Gardenia carinata* shell.

The objective of this study is to examine the dye removal efficiency of AC derived from *Gardenia carinata*, to examine the interactive influence of process variables and to investigate the mass transfer resistance of methylene blue (MB) on *Gardenia carinata* activated carbon (GCAC).

2. Experimental

2.1. Adsorbate preparation

A 1,000 ppm stock solution of methylene blue (MB) was prepared using C:I:52015 dye and various working concentrations (20, 40, 60 mg/L) were prepared through dilution. The maximum wavelength of MB adsorbance was obtained at 662 nm using a spectrophotometer (DR 2000).

2.2. Adsorbent preparation

Gardenia carinata seeds were collected from Tronoh, Perak, Malaysia. The seeds were broken and the shells were cleaned using 2% HNO_3. The shells were washed severally to eliminate impurities and dried at 120°C for 24 h to eliminate moisture. Pyrolysis of dried *Gardenia carinata* shell was conducted at 400°C using a muffle furnace for 2 h. The char was washed several times with distilled water and impregnated with H_3PO_4 in the ratio of 1:2 (char: H_3PO_4). The mixture was thoroughly mixed for 5 h and re-dried at 120°C for 24 h. The H_3PO_4 treated char was placed in a boat-shaped cylindrical ceramic dish and fitted in a tube furnace operated with a 99.9% high purity nitrogen at a flow rate of 100 cm/min until final temperature of 800°C. The heating was conducted at 20°C/min and the char was activated for 2 h. Nitrogen gas was intermittently used during heating and cooling process but was replaced with CO_2 during the activation process (2 h). After activation and cooling, the products were washed several times using deionized water to achieve a final pH of 6–7. The products were dried at 120°C for 24 h and finally sieved to obtain an adsorbent with particle size of about 30–125 μm. The adsorbent was termed *Gardenia carinata* activated carbon (GCAC).

2.3. Adsorbent characterization

GCAC micrograph was obtained using Zeiss supra scanning electron microscope (Germany). The functional groups on GCAC were examined using a Fourier transform infrared spectroscopy. The surface area of GCAC was characterized using BET method.

2.4. Mass transfer kinetics

The batch experiments were conducted by placing different concentrations (20, 40 and 60 mg/L) of 100 mL MB solution in a 150 mL conical flask. Various mass of GCAC was added into the flask. The flask was agitated in a water bath operated at 298 K for 300 min until equilibrium was attained. Treated MB solutions were collected and analyzed at various intervals. The percentage of MB removal was calculated using the expression:

$$E = \frac{C_0 - C_s}{C_0} \tag{1}$$

where E, C_0 and C_s are MB removal (%), initial concentration and concentration at any time (mg/L), respectively.

The total amount of MB adsorbed on GCAC at a given MB concentration can be calculated using the expression [33] as follows:

$$q = \int_0^V \frac{\left(C_0 - C_s\right)}{m} \times dV \tag{2}$$

q represents the cumulative amount of adsorbate sorbed onto the adsorbent material (mg/g), V represents the quantity of treated sample (L) and m represents the adsorbent mass (g).

Application of the linearized modified mass transfer factor (MMTF) model can give an understanding of the mass

transfer of MB onto GCAC. The linearized expression of MMTF is [33,34] as follows:

$$\ln(q) = \frac{1}{\beta} \times \ln(t) + B \tag{3}$$

$$B = \frac{\ln\left(\left[k_L a\right]_g\right) - \ln\left\{\ln\left(\frac{C_0}{C_s}\right)\right\}}{\beta} \tag{4}$$

B represents the mass transfer index related to driving force (mg/g), β represents attraction of the adsorbent and the adsorbate (g/h/mg), t represents reaction time.

Variation of the adsorbate concentration relative to time can be expressed as [35] follows:

$$\frac{dC/C_0}{d_t} - k_f A \tag{5}$$

where C represents solute concentration at any time t, k_f represents external mass transfer constant (cm/s), A represents adsorbent surface area per unit volume (m^{-1}) expressed as follows:

$$A = \frac{6M}{Vd_p P\left(1-\varepsilon_p\right)} \tag{6}$$

where ε_p is bed porosity and r is bulk density (g/cm^3).

The transport of MB onto GCAC and into the acceptor sites of the adsorbent can be controlled by different transport mechanisms. The intraparticle diffusion model accounts for solute transport across a boundary layer and can be linearly expressed as [36] follows:

$$q_t = k_{\text{id}} t^{0.5} + C_i \tag{7}$$

where q_t represents the quantity of adsorbed adsorbate at any time (mg/g), k_{id} represents intraparticle diffusion rate constant (mg $min^{0.5}$), C_i represents the boundary layer thickness (mg/g).

2.5. pH point of zero charge

To understand charge distribution on the adsorbent and the point of neutrality, the pH point of zero charge (pH_{PZC}) of GCAC was determined by equilibrating 0.1 g of GCAC in NaCl (0.1 M) at 25°C ± 1°C for 24 h. The pH values were varied from 2 to 12 and were controlled using NaOH or H_2SO_4 (0.1 M). After equilibration, the final pH of the settled samples was obtained using a pH meter (Sension^{tm} pH meter). The pH_{PZC} was then obtained by subtracting the initial pH from the final pH and plotting the difference vs. initial pH.

2.6. Statistical design of experiment

The experiments were designed using the central composite design (CCD) model of RSM. The effect of three parameters (pH, concentration and adsorbent mass) on the response (methylene blue) was evaluated by the model. Each parameter was varied across five levels and three different points (axial, factorial and center points). Numeric variation of the parameters show the low, center and high regions of the model design space. The independent variables are shown in Table 1. From the combination of the three variables across five levels, the software generated a total of 20 experimental runs with five replicate experiments at the center points.

The batch study was carried out according to the combination of the variables in the model. A 150 mL flask containing 100 mL MB solution was used for each experimental run. The flask was placed in a water bath at 298 K for a pre-determined reaction time of 30 min. After each experimental run, supernatants were withdrawn from the settled samples to measure residual MB concentration.

3. Results and discussion

3.1. GCAC surface area

Evaluation of GCAC characteristics shows that it has a high surface area (Table 2). This indicates that *Gardenia carinata* is a suitable waste material for AC production.

The BET surface area for char and GCAC differed. The surface area of GCAC and char were 1,187.33 m^2/g and 435.55 m^2/g, respectively. This implies that activation and carbonization caused enlargement of the surface area of GCAC. Furthermore, micropore area and external surface area for GCAC were higher than char (Table 2). Table 3 compares GCAC with other ACs derived from agricultural waste. It was observed that *Gardenia carinata* is a suitable waste material for AC production based on the surface area of GCAC.

3.2. FTIR spectroscopy

The functional groups on GCAC and MB-loaded GCAC were examined and presented in Table 4. The peaks between 615 and 619/cm represent –C≡C–H bend alkyne groups. Strong C–H spectra of aromatic groups were found between 873 and 873.09/cm. The peaks at 1,113.71 and 1,422/cm on GCAC represents carboxylic acid and medium C–C stretch aromatic groups. These two peaks

Table 1
CCD experimental parameters

Level	–1	0	+1	Code
pH	4	7	10	*A*
MB concentration	20 mg/L	40 mg/L	60 mg/L	*B*
GCAC	0.03 g	0.06 g	0.09 g	*C*

Table 2
GCAC BET characteristics

Parameters	Char	GCAC
BET surface area (m^2/g)	435.55	1,187.33
Micropore area (cm^3/g)	349.59	785.69
External surface area (cm^3/g)	85.963	247.11

Table 3
Comparison of surface area of various adsorbents

Precursor	BET surface area (m^2/g)	Reference
Oil palm fiber	707.79	[8]
Empty fruit bunch	749–928	[37]
Palm kernel shell	205.86	[38]
Mesocarp fiber	239.50	[38]
Oil palm wood	931.6	[39]
Palm oil fruit shell	37.98	[40]
Palm oil mill sludge	87.1	[41]
Pistachio shell	635	[42]
Almond shell	1,208	[42]
Hazelnut shell	786	[42]
Walnut shell	941	[42]
Apricot shell	861	[42]
GCAC	1,187.33	Present study

Table 4
GCAC and MB-loaded GCAC FTIR characteristics

GCAC (cm^{-1})	MB-loaded GCAC (cm^{-1})	Functional groups
615	619	–C≡C–H alkyne
873	873.09	C–H aromatic
1,113.71	–	Carboxylic acid
1,422	–	C–C aromatic
1,618.30	1,617.47	N–H amine
1,637.06	1,637.5	N–H amine
3,413.5	3,412.82	O–H, alcohols and phenols
3,465.86	3,473.89	O–H, alcohols and phenols
3,542.6	3,546.2	O–H, alcohols and phenols

disappeared in MB-loaded GCAC due to the interaction of the adsorbent and adsorbate. The bend between 1,618 and 1,637/cm indicates medium strength N–H amine groups. The stretch between 3,413.5; 3,465.86 and 3,542.6/cm represents strong and bend O–H, H–bonded alcohols and phenols. A significant shift, disappearance and broadening of peaks were observed on the MB-loaded GCAC due to the coalescing of the functional groups of GCAC with the active groups of the adsorbate.

3.3. SEM micrographs

Fig. 1 shows the SEM micrographs of char and GCAC. The micrograph for char was cloudy with less porosity (Fig. 1a) while GCAC showed an even distribution of pores and active sites (Fig. 1b). GCAC is porous, indicating its capacity to adsorb more dye molecules.

3.4. Model analysis

The data obtained from the 20 experimental runs analyzed by the CCD model could be fitted into the second order polynomial equation as follows:

$$Y = \beta_0 + \sum_{j=1}^{k} \beta_j x_j + \sum_{j=1}^{k} \beta_{jj} x^2 j + \sum \sum_{i<j=2} \beta_{ij} x_i x_j + e_i \quad (8)$$

where Y represents response, x_i and x_j represent parameters, β_0 represent constant factor, β_j, β_{jj}, β_{ij} represent interaction constants (linear, quadratic, second order terms), k represents number of evaluated factors, e_i represents error.

The process parameters in their coded values can be explained using the expression

$$x_i = \frac{x_i - x_0}{\Delta x_i} \quad (9)$$

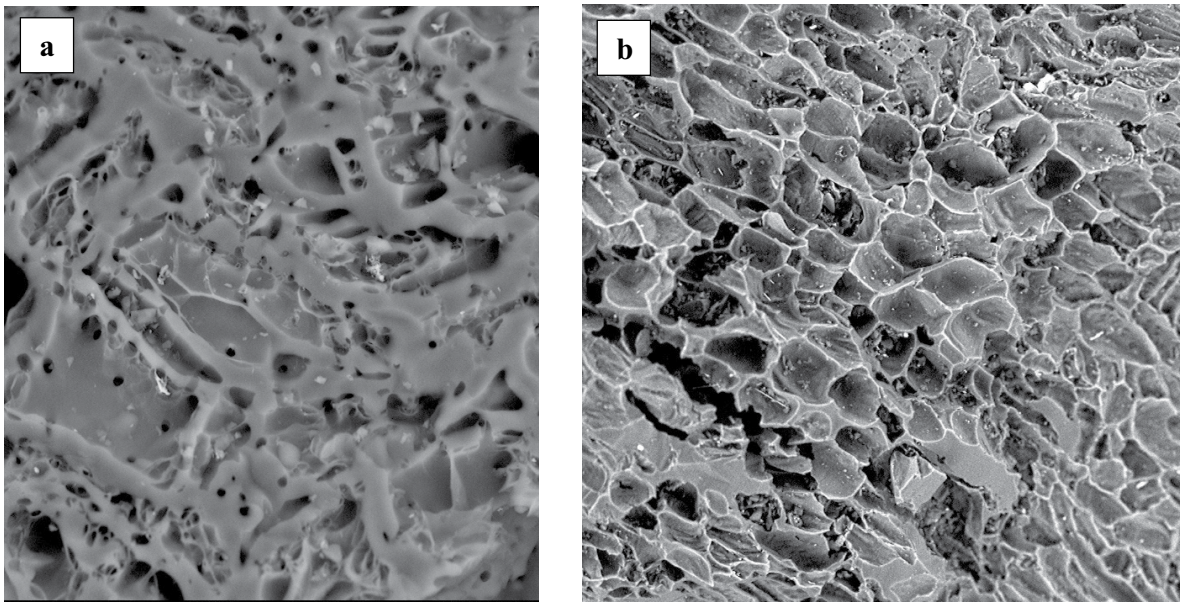

Fig. 1. SEM micrographs of (a) char and (b) GCAC.

where x_i represents uncoded value, x_0 represents uncoded value at center point, Δx_i represents the change value (–1 and +1).

The interaction between the independent variables was examined by ANOVA. The significance of the model was determined by *F*-test and correlation coefficient (R^2). The model terms were verified by the *P*-value at 95% confidence level. Finally, 3D plots were obtained.

3.5. ANOVA analyses

The significant model terms of the regression variables were evaluated by ANOVA. The model was significant with *F*-value of 22.58 and Prob > F < 0.0001. For any significant model, the Prob > F value must be <0.0500. Therefore the model obtained in this study is significant and indicates that CCD can be used to model MB adsorption onto GCAC.

3.5.1. Signal to noise ratio

The signal to noise ratio of the CCD model was evaluated using the adequate precision (AD) matrix. AD compares the estimated values to the average estimated error. AD values higher than 4 is required for a good model. The AD obtained in this study was 16.252, implying that the model possesses adequate signal for optimization.

3.5.2. Correlations

The CCD model of RSM generates three different correlation coefficients (R^2, predicted R^2 and adjusted R^2). These coefficients are used to examine model adequacy. Predicted R^2 evaluates the suitability of the model to predict a response value. The model is in reasonable agreement if the difference between the adjusted and predicted R^2 is <0.2. In this study, the predicted R^2 was 0.7526 while the adjusted R^2 was 0.9109 (difference of 0.1583), indicating that the model fitted well. The correlation coefficient (R^2) describes the alignment of the response to the model. For a good model, a value of R^2 higher than 0.80 is ideal. The R^2 obtained in this study was 0.9531. This indicates that the model has a goodness of fit. The coefficient of variation (CV) evaluates model reproducibility. Normal values of CV are less than 10% [43]. The CV value of 3.89 obtained in this study implies that the model is reproducible.

3.5.3. Lack of fit

The lack of fit is related to the residual and pure error. Unaccounted variations within the model can influence both residual and pure error and produce a significant lack of fit. For any good RSM model, a non-significant lack of fit is desirable. The lack of fit in this study is non-significant with F-value of 1.02, indicating that the model was suitable for MB adsorption.

3.5.4. Standard deviation

The standard deviation is related to the experimental error within the design space. A low standard deviation is desirable and related to the square root of the residual mean square. A standard deviation of 2.94 obtained in this study is in agreement with the model.

3.5.5. Predicted model

The significant terms obtained from the model is summarized in Table 5. The degree of freedom (DF) of these significant model terms is 1. This indicates that the model used for MB adsorption onto GCAC was significant. The regression model representing the coded factors can be described by the second order polynomial:

$$\mathrm{MB} = +80.3 + 2.7A - 2.5B + 7.5C + 3.05A^2 - 6.5B^2 - 5.6C^2 - 2.3AB + 0.7AC + 8.7BC \quad (10)$$

The second order polynomial in Eq. (10) shows the interaction of the variables and their order of significance within the design space. The order of the significance of the variables is pH > adsorbent mass > MB concentration.

Diagnostic plots were used to examine the adequacy of the model to navigate the design space. The normal probability plot in Fig. 2a shows evenly distributed parallel residuals along a straight line. This indicates that the model satisfactorily fitted with the experimental data. The plot in Fig. 2b shows that the residual points of both estimated and actual data were closely aligned on opposite trajectory on the straight line, indicating that the model prediction of MB adsorption on GCAC was satisfactory.

3.6. MB removal

The influence of pH could be related to the pH point of zero charge (pH_{PZC}). GCAC has a pH_{PZC} of 8.1. This indicates that GCAC surface has positive and negative charges below and above 8.1, respectively. GCAC has functional groups such as OH, CO and CH which can dissociate into separate smaller ions and protonate with the adsorbate molecules, eliminating more adsorbate molecules from the aqueous solution. The higher MB removal at pH 4 (Fig. 3a) could be related to GCAC functional group dissociation and protonation with MB molecules. Table 3 shows that the functional groups on GCAC interacted with MB molecules. The O–H group on GCAC significantly interacted with the MB molecules in such a way that altered its band width. The O–H groups at 3,413.5; 3,465.86 and 3,542.6/cm on GCAC shifted to 3,412.82; 3,473.89 and 3,546.2/cm, respectively, in the MB-loaded GCAC due to their interaction with MB

Table 5
ANOVA significant model terms

Model	F-value	Prob > F
A	8.6	0.015
B	7.2	0.023
C	64.5	0.0001
B^2	13.5	0.004
C^2	10	0.01
BC	70	0.001

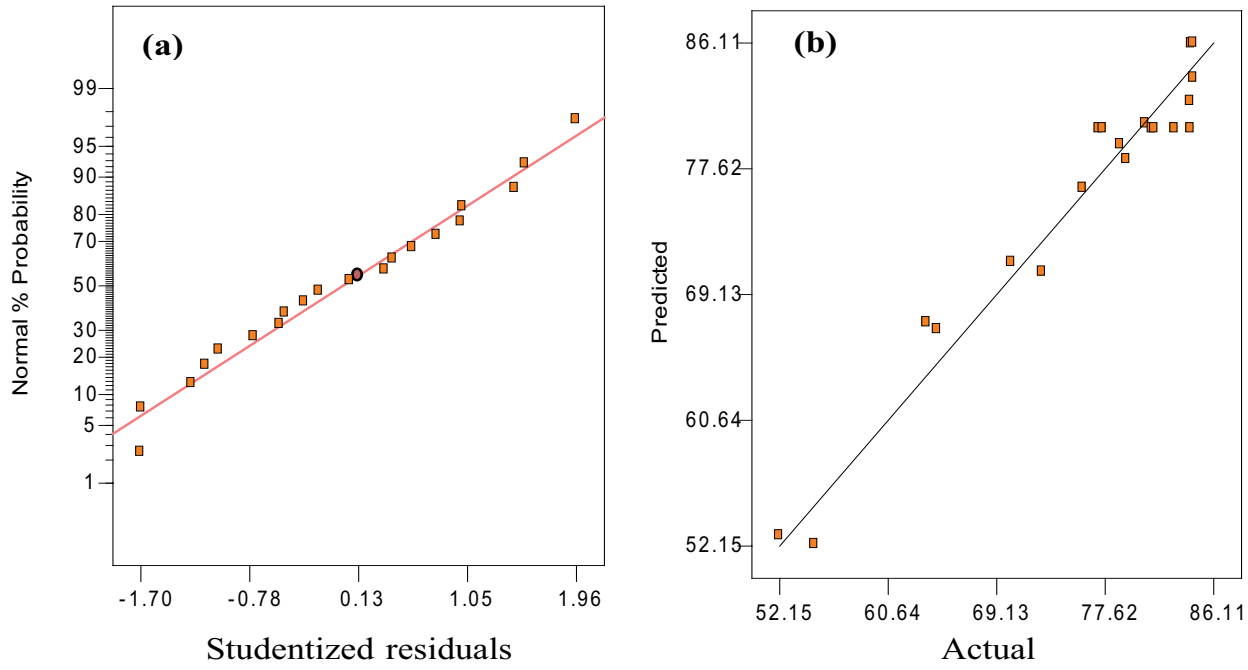

Fig. 2. Diagnostic plots (a) normal probability plot and (b) predicted vs. actual plot.

molecules. The carboxylic acid and C–C aromatic groups on GCAC were found at band width of 1,113.71 and 1,422/cm, respectively, but completely disappeared on the MB-loaded GCAC. Therefore, lower pH enhanced the protonation of GCAC functional groups, attracting more MB molecules. This observation is in line with other reports [10,44].

The influence of initial concentrations (20, 40 and 60 mg/L) on MB adsorption was examined at various adsorbent mass. The results show that MB removal percentage was higher at lower concentration. MB removal percentage at 20 mg/L was 89% but decreased to 79% when initial concentration was elevated to 60 mg/L (Fig. 3a). This phenomenon could be due to higher active sites on GCAC at low initial MB concentration. The active sites on GCAC were sufficient for the adsorbate at low concentration. At higher concentration and at the same adsorbent mass, the active sites could be insufficient to adsorb more MB molecules. However, MB uptake was higher with increasing MB concentration. An uptake of 25.3, 55.4 and 70.3 mg/g was noted with elevating MB concentrations from 20, 40 and 60 mg/L, respectively. The results show that the driving force of MB transport onto GCAC was higher at elevated MB concentration. At higher MB concentration, higher mass transfer from GCAC surface into the micropore occurs due to higher driving force of the adsorbate [45]. This observation is in line with other reports [45].

The influence of adsorbent mass on MB adsorption is presented in Fig. 3b. Higher adsorbent mass of 0.09 g adsorbed more dye molecules than lower adsorbent mass of 0.03 g. At lower adsorbent mass, the active sites could be rapidly filled by adsorbate while high amount of solute remains in the aqueous solution. At lower adsorbent mass, MB removal percentage on GCAC decreased but increased when adsorbent mass was increased due to the

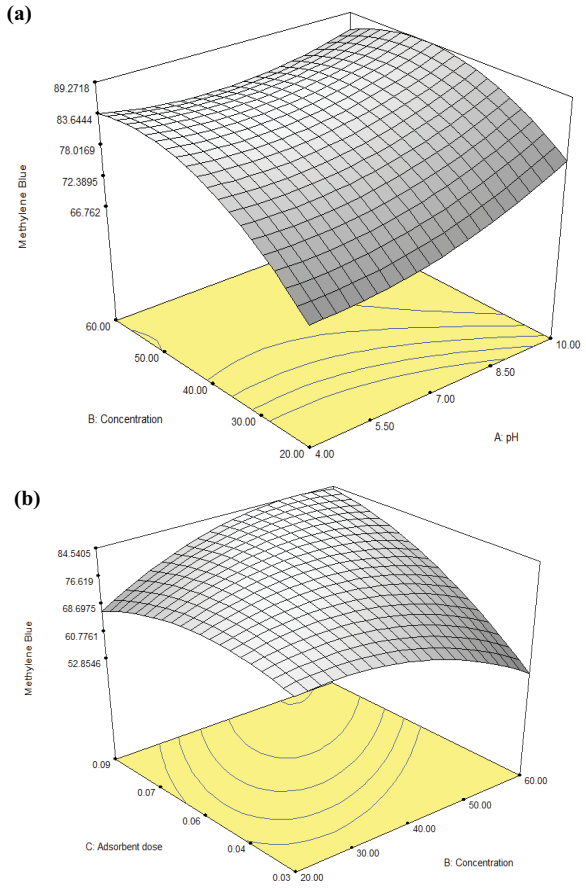

Fig. 3. (a) Effect of pH and concentration and (b) effect of adsorbent mass.

availability of adequate active sites. In contrast, MB uptake on GCAC reduced at higher adsorbent mass. The MB uptake at adsorbent mass of 0.03 and 0.09 g was 53 and 18 mg/g, respectively. Thus, more MB uptake was observed at lower adsorbent mass per unit volume. This observation is in line with previous reports [46].

3.7. Optimization

Optimization of MB adsorption onto GCAC was conducted using RSM software. A goal for each of the three variables and the response was set, respectively. The goal for the variables was set to maximum in order to capture the optimum region while the response was set "within range". RSM combines individual desirabilities into one number and identifies the optimum regions, conditions and removal efficiency.

Table 6 shows the optimization of MB removal in this study. RSM predicted MB removal of 89.2% at pH of 4.3, concentration of 51 mg/L and adsorbent mass of 0.08 g. The corresponding experimental investigation yielded a removal efficiency of 92.3%, confirming that the model prediction was reasonably optimized.

4. Mass transfer kinetics

To understand an adsorption mechanism, investigation into the liquid–solid interaction is necessary. The transport of adsorbate in aqueous solution can be influenced by various factors including adsorbate concentration, adsorbate solubility, adsorbent functional groups, surface area and porosity. Several mechanisms including chemical bonding, covalent bonding and interactions of the functional groups with the solute can influence the adsorbate–adsorbent affinity [30]. Therefore the transfer of solute onto a porous solid could primarily involve external mass transport, intraparticle diffusion and active site adsorption [47].

Table 6
MB numerical optimization

pH	4.3
Concentration (mg/L)	51
Adsorbent mass (g)	0.08
Predicted MB (%)	89.2
Experimental MB (%)	92.3
Desirability	1.000

4.1. Adsorbate–adsorbent affinity

Several reaction mechanisms control the mass transfer of solutes onto the active sites of a porous solid. The net transfer of mass and the resistance to solute transport can be examined using various established and modified mass transfer kinetic models. The linear form of the MMTF model developed by Fulazzaky [30] (Eqs. (3) and (4)) can be used to understand the attraction of the adsorbate toward the adsorbent and the driving force of adsorbate mass transfer. The plot of ln q vs. ln t provides a slope representing 1/β and intercept of B. Fig. 4 shows that the mass transfer of MB onto GCAC was greater at higher MB concentration (Table 7). This indicates that there was no mass transfer resistance with increasing solute concentration.

The driving force of MB mass transfer onto GCAC increased in the range of 3.621, 4.387 and 4.906 mg/g with increasing concentration in the range of 20, 40 and 60 mg/L, respectively. Similarly, the attraction of the adsorbate toward

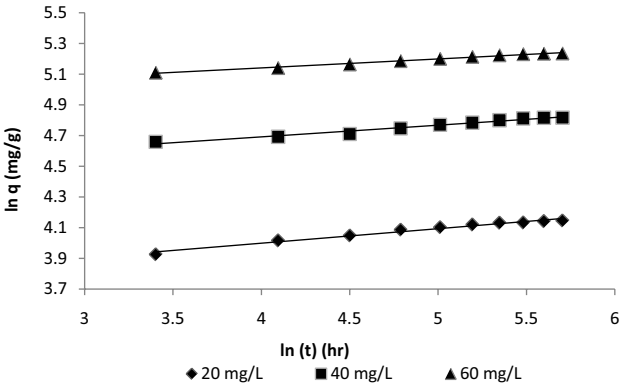

Fig. 4. Mass transfer plot of ln q vs ln t.

Table 7
Mass transfer coefficients of different models

		mg/L		
Models	Constants	20	40	60
Mass transfer coefficients:	β (g/h/mg)	10.570	13.123	17.064
ln q vs. ln t	B (mg/g)	3.621	4.387	4.906
	R^2	0.9785	0.9747	0.9913
External mass transfer coefficients:	k_f (cm/s)	1.04×10^{-3}	1.34×10^{-3}	1.57×10^{-3}
C_t/C_0 vs. t	R^2	0.9236	0.9797	0.9754
Intraparticle diffusion model:	K_{id} (mg min)$^{0.5}$	0.992	2.6602	1.9513
q_t vs. $t^{0.5}$	C_i (mg/g)	47.41	96.62	156.44
	R^2	0.9236	0.9797	0.9754

the adsorbent (β) increased in the range of 10.57, 13.123 and 17.064 g/h/mg with increasing MB concentration. The higher driving force of MB at higher concentration caused the mass transfer of large amount of solute onto the adsorbent. The correlation coefficient at all examined initial MB concentrations was high and exceeded 0.96, indicating the applicability of this model. These findings are in line with the study of Fulazzaky et al. [48] on the biosorption of oil and grease by *Serratia marcescens* SA30. The authors found that β and *B* increased with increasing initial oil and grease concentration.

4.2. External mass transfer

Evaluation of the transport of MB onto the external pores of the adsorbent can be conducted through the plot of C_t/C_0 vs. t [35]. Table 7 shows the external mass transfer factors at different MB concentration. The k_f increased in the range of 1.04×10^{-3}–1.57×10^{-3} with increasing concentrations from 20 to 60 mg/L. For all MB concentration, correlation coefficient was high (>0.992). The result suggests that higher initial solute concentration caused an increase of external mass transfer onto the surface of the adsorbent. This further indicates that there was no mass transfer resistance of MB onto GCAC. A related study by Souza et al. [47] noted that external mass transfer (k_f) values increased with increasing malachite green (MG) concentrations. The researchers found that k_f was in the range of 1.99, 2.16, 2.44, 2.65 and 2.89 cm/s when MG concentration was raised to 150, 200, 250, 300 and 500 mg/L, respectively.

4.3. Intraparticle diffusion

The transport of solute can be explained by the linearized expression of the Weber and Morris intraparticle diffusion model of ln q_t vs. $t^{0.5}$. Reactions controlled by intraparticle diffusion must fulfill the following criteria [49]:

- The plot of ln q_t vs. $t^{0.5}$ must pass through the origin
- The boundary layer effect (C_i) must be low

The intraparticle diffusion plot in Fig. 5 deviated from the origin. The k_{id} was high (0.992–1.9513 mg (min)$^{0.5}$) as well as the correlation coefficient (R^2). However, the boundary layer effect (C_i) was high and increased with increasing initial MB concentration (Table 7). The high C_i indicates the presence of a great boundary layer effect [50]. Lower values of C_i favor intraparticle diffusion. The departure of the plot from the origin indicates that intraparticle diffusion was not the only transport mechanism but more than one transport mechanism could be involved in the transfer of MB onto GCAC [51]. A similar observation was made by Kapur and Mondal [52] who found that the k_{id} value increased to 0.038, 0.119 and 0.601 mg/g min$^{-1/2}$ with increasing Cr(VI) concentration from 10 to 20 and 50 mg/L, respectively. Walker et al. [53] also demonstrated that k_{id} increased in the range of 0.98, 1.93, 3.77 and 5.41 mg min$^{0.5}$ with increasing dye concentration to 400, 600, 800 and 1,000 mg/L, respectively.

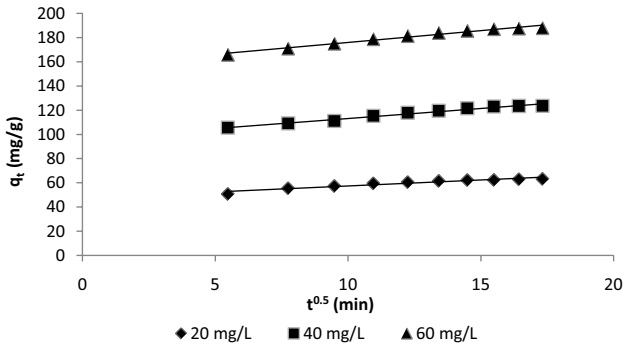

Fig. 5. Intraparticle diffusion model.

5. Conclusion

AC derived from *Gardenia carinata* (GCAC) was examined for MB adsorption from aqueous solution. The adsorbent has high BET surface area. The experiments were designed using the CCD model of RSM. The influence of three independent variables (pH, adsorbent mass and concentration) on MB adsorption was evaluated. It was found that the variables influenced MB adsorption. MB adsorption of 89% was achieved at pH 4 and adsorbent mass of 0.06/g. The model was satisfactorily optimized. The mass transfer analyses indicated that the attraction of the adsorbate toward the adsorbent was influenced by MB concentrations. The external mass transfer factor (k_f) showed that there was no mass transfer resistance of MB onto GCAC. Furthermore, mass transfer analyses indicated that the transport of the solute onto GCAC could be governed by both intraparticle diffusion and film diffusion. This study, therefore, demonstrates that waste materials such as *Gardenia carinata* seeds can be effectively reused in more benefitting ways.

Acknowledgments

The authors are grateful to Universiti Teknologi PETRONAS where this study was conducted. They are also thankful to the laboratory technician Mr. Mohd Khairul Anuar Jamaluddin for his assistance.

References

[1] P.N. Dave, S. Kaur, E. Khosla, Removal of Eriochrome black-T by adsorption on to eucalyptus bark using green technology, Indian J. Chem. Technol., 18 (2011) 53–60.
[2] Z. Carmen, S. Daniela, Textile Organic Dyes–Characteristics, Polluting Effects and Separation/Elimination Procedures from Industrial Effluents–A Critical Overview, Intechopen Publications, London, 2012,p. 54–86.
[3] C. Pearce, J.R. Lloyd, J.T. Guthrie, The removal of colour from textile wastewater using whole bacterial cells: a review, Dyes Pigm., 58 (2003) 179–196.
[4] N. Barka, M. Abdennouri, M.E.L. Makhfouk, Removal of Methylene Blue and Eriochrome Black T from aqueous solutions by biosorption on *Scolymus hispanicus L.*: kinetics, equilibrium and thermodynamics, J. Taiwan Inst. Chem. Eng., 42 (2011) 320–326.
[5] P.A. Carneiro, G.A. Umbuzeiro, D.P. Oliveira, M.V.B. Zanoni, Assessment of water contamination caused by a mutagenic textile effluent/dyehouse effluent bearing disperse dyes, J. Hazard. Mater., 174 (2010) 694–699.
[6] R.O.A. de Lima, A.P. Bazo, D.M.F. Salvadori, C.M. Rech, D. de Palma Oliveira, G. de Aragão Umbuzeiro, Mutagenic

and carcinogenic potential of a textile azo dye processing plant effluent that impacts a drinking water source, Mutat. Res. Genet. Toxicol. Environ. Mutagen., 626 (2007) 53–60.
[7] D. Rawat, V. Mishra, R.S. Sharma, Detoxification of azo dyes in the context of environmental processes, Chemosphere, 155 (2016) 591–605.
[8] K.Y. Foo, B.H. Hameed, Microwave-assisted preparation of oil palm fiber activated carbon for methylene blue adsorption, Chem. Eng. J., 166 (2011) 792–795.
[9] S. Sadaf, H. Bhatti, S. Nausheen, S. Noreen, Potential use of low-cost lignocellulosic waste for the removal of Direct Violet 51 from aqueous solution: equilibrium and breakthrough studies, Arch. Environ. Contam. Toxicol., 66 (2014) 557–571.
[10] S. Noreen, H.N. Bhatti, Fitting of equilibrium and kinetic data for the removal of Novacron Orange P-2R by sugarcane bagasse, J. Ind. Eng. Chem., 20 (2014) 1684–1692.
[11] S. Sadaf, H. Bhatti, Evaluation of peanut husk as a novel, low cost biosorbent for the removal of Indosol Orange RSN dye from aqueous solutions: batch and fixed bed studies, Clean Technol. Environ. Policy, 16 (2014) 527–544.
[12] S. Nausheen, H.N. Bhatti, Z. Furrukh, S. Sadaf, S. Noreen, Adsorptive removal of Drimarine Red HF-3D dye from aqueous solution using low-cost agricultural waste: batch and column study, Chem. Ecol., 30 (2014) 376–392.
[13] B.H. Hameed, A.T.M. Din, A.L. Ahmad, Adsorption of methylene blue onto bamboo-based activated carbon: kinetics and equilibrium studies, J. Hazard. Mater., 141 (2007) 819–825.
[14] A.L. Cazetta, A.M.M. Vargas, E.M. Nogami, M.H. Kunita, M.R. Guilherme, A.C. Martins, T.L. Silva, J.C.G. Moraes, V.C. Almeida, NaOH-activated carbon of high surface area produced from coconut shell: Kinetics and equilibrium studies from the methylene blue adsorption, Chem. Eng. J., 174 (2011) 117–125.
[15] M.Z. Alam, S.A. Muyibi, M.F. Mansor, R. Wahid, Activated carbons derived from oil palm empty-fruit bunches: application to environmental problems, J. Environ. Sci., 19 (2007) 103–108.
[16] A.M. Faizal, S.R.M. Kutty, E.H. Ezechi, Modelling of Adams-Bohart and Yoon-Nelson on the removal of oil from water using microwave incinerated rice husk ash (MIRHA), Appl. Mech. Mater., 625 (2014) 788–791.
[17] S.R.M. Kutty, E.H. Ezechi, S.G. Khaw, C.L. Lai, M.H. Isa, Evaluation of copper removal using MIRHA as an adsorbent in a continuous flow activated sludge system, Water Pollut. XII, 182 (2014) 233–244.
[18] S. Kutty, E. Ezechi, S. Khaw, C. Lai, M. Isa, Comparison of the effect of two support materials on copper removal from aqueous solution in the activated sludge process, Energy and Sustainability V: Special Contrib., 206 (2015) 149–159.
[19] V. Ponnusami, R. Aravindhan, N. Karthik Raj, G. Ramadoss, S. Srivastava, Adsorption of methylene blue onto gulmohar plant leaf powder: equilibrium, kinetic, and thermodynamic analysis, J. Environ. Prot. Sci., 3 (2009) 1–10.
[20] E.H. Ezechi, S.R. bin Mohamed Kutty, A. Malakahmad, M.H. Isa, N. Aminu, I.U. Salihi, Removal of methylene blue from dye effluent using ageratum conyzoide leaf powder (ACLP), AIP Conf. Proc., 1669 (2015) 020013.
[21] E.H. Ezechi, S.R. bin Mohamed Kutty, A. Malakahmad, I.U. Salihi, N. Aminu, Determination of optimum range for hexavalent chromium Cr (VI) removal using ageratum conyzoide leaf powder (ACLP), AIP Conf. Proc., 1669 (2015) 020014.
[22] K.G. Bhattacharyya, A. Sharma, Kinetics and thermodynamics of Methylene Blue adsorption on Neem (i-Azadirachta indica) leaf powder, Dyes Pigm., 65 (2005) 51–59.
[23] S.K. Behera, H. Meena, S. Chakraborty, B. Meikap, Application of response surface methodology (RSM) for optimization of leaching parameters for ash reduction from low-grade coal, Int. J. Min. Sci. Technol., 28 (2018) 621–629.
[24] E.H. Ezechi, M.H. Isa, S.R. bin Mohamed Kutty, Z. Ahmed, Electrochemical removal of boron from produced water and recovery, J. Environ. Chem. Eng., 3 (2015) 1962–1973.
[25] M. Amini, H. Younesi, N. Bahramifar, A.A.Z. Lorestani, F. Ghorbani, A. Daneshi, M. Sharifzadeh, Application of response surface methodology for optimization of lead biosorption in an aqueous solution by Aspergillus niger, J. Hazard. Mater., 154 (2008) 694–702.
[26] J.L. Pilkington, C. Preston, R.L. Gomes, Comparison of response surface methodology (RSM) and artificial neural networks (ANN) towards efficient extraction of artemisinin from Artemisia annua, Ind. Crops Prod., 58 (2014) 15–24.
[27] E.H. Ezechi, S.R.b. M. Kutty, M.H. Isa, M.S. Liew, Application of response surface methodology for the optimization of hexavalent chromium removal using a new low-cost adsorbent, Desal. Wat. Treat., 57 (2016) 22507–22518.
[28] D. Fu, Y. Zhang, F. Lv, P.K. Chu, J. Shang, Removal of organic materials from TNT red water by bamboo charcoal adsorption, Chem. Eng. J., 193 (2012) 39–49.
[29] C. Yao, T. Chen, A film-diffusion-based adsorption kinetic equation and its application, Chem. Eng. Res. Des., 119 (2017) 87–92.
[30] M.A. Fulazzaky, Determining the resistance of mass transfer for adsorption of the surfactants onto granular activated carbons from hydrodynamic column, Chem. Eng. J., 166 (2011) 832–840.
[31] O. Zongram, N. Ruangrungsi, K. Rungsihirunrat, RAPD fingerprinting and genetic relationship of Gardenia species in Thailand, Songklanakarin J. Sci. Technol., 39 (2017) 471–477.
[32] E.H. Ezechi, M.H. Isa, S.R. Kutty, N.B. Sapari, Boron Recovery, Application and Economic Significance: A Review, National Postgraduate Conference (NPC) Perak, Malaysia, 19–20 September 2011, IEEE ISBN 978-1-4577-1882-3, pp. 815–820.
[33] M.A. Fulazzaky, M. Nuid, A. Aris, K. Muda, Kinetics and mass transfer studies on the biosorption of organic matter from palm oil mill effluent by aerobic granules before and after the addition of Serratia marcescens SA30 in a sequencing batch reactor, Process Saf. Environ. Prot., 107 (2017) 259–268.
[34] M.A. Fulazzaky, M.H. Khamidun, R. Omar, Understanding of mass transfer resistance for the adsorption of solute onto porous material from the modified mass transfer factor models, Chem. Eng. J., 228 (2013) 1023–1029.
[35] C.R. Girish, V.R. Murty, Mass transfer studies on adsorption of phenol from wastewater using Lantana camara, forest waste, Int. J. Chem. Eng., 2016 (2016) 11. http://dx.doi.org/10.1155/2016/5809505.
[36] H.K. Boparai, M. Joseph, D.M. O'Carroll, Kinetics and thermodynamics of cadmium ion removal by adsorption onto nano zerovalent iron particles, J. Hazard. Mater., 186 (2011) 458–465.
[37] T. Lee, Z.A. Zubir, F.M. Jamil, A. Matsumoto, F.-Y. Yeoh, Combustion and pyrolysis of activated carbon fibre from oil palm empty fruit bunch fibre assisted through chemical activation with acid treatment, J. Anal. Appl. Pyrolysis, 110 (2014) 408–418.
[38] N.S.A. Wafti, H.L.N. Lau, S.K. Loh, A.A. Aziz, Z. Ab Rahman, C.Y. May, Activated carbon from oil palm biomass as potential adsorbent for palm oil mill effluent treatment, J. Oil Palm Res., 29 (2017) 278–290.
[39] A. Ahmad, M. Loh, J. Aziz, Preparation and characterization of activated carbon from oil palm wood and its evaluation on methylene blue adsorption, Dyes Pigm., 75 (2007) 263–272.
[40] M.A. Hossain, H.H. Ngo, W.S. Guo, T.V. Nguyen, Palm oil fruit shells as biosorbent for copper removal from water and wastewater: experiments and sorption models, Bioresour. Technol., 113 (2012) 97–101.
[41] S. Thangalazhy-Gopakumar, W.M.A. Al-Nadheri, D. Jegarajan, J.N. Sahu, N.M. Mubarak, S. Nizamuddin, Utilization of palm oil sludge through pyrolysis for bio-oil and bio-char production, Bioresour. Technol., 178 (2015) 65–69.
[42] M. Kazemipour, M. Ansari, S. Tajrobehkar, M. Majdzadeh, H.R. Kermani, Removal of lead, cadmium, zinc, and copper from industrial wastewater by carbon developed from walnut, hazelnut, almond, pistachio shell, and apricot stone, J. Hazard. Mater., 150 (2008) 322–327.
[43] M.O. Saeed, K.A.M. Azizli, M.H. Isa, E.H. Ezechi, Treatment of POME using Fenton oxidation process: removal efficiency, optimization, and acidity condition, Desal. Wat. Treat., 57 (2016) 23750–23759.

[44] H. El Boujaady, M. Mourabet, M. Bennani-Ziatni, A. Taitai, Adsorption/desorption of Direct Yellow 28 on apatitic phosphate: mechanism, kinetic and thermodynamic studies, J. Assoc. Arab Univ. Basic Appl. Sci., 16 (2014) 64–73.
[45] M. Ghaedi, A. Ansari, M.H. Habibi, A.R. Asghari, Removal of malachite green from aqueous solution by zinc oxide nanoparticle loaded on activated carbon: kinetics and isotherm study, J. Ind. Eng. Chem., 20 (2014) 17–28.
[46] M. Roosta, M. Ghaedi, A. Daneshfar, S. Darafarin, R. Sahraei, M.K. Purkait, Simultaneous ultrasound-assisted removal of sunset yellow and erythrosine by ZnS: Ni nanoparticles loaded on activated carbon: optimization by central composite design, Ultrason. Sonochem., 21 (2014) 1441–1450.
[47] P.R. Souza, G.L. Dotto, N.P.G. Salau, Statistical evaluation of pore volume and surface diffusion model in adsorption systems, J. Environ. Chem. Eng., 5 (2017) 5293–5297.
[48] M.A. Fulazzaky, S. Abdullah, M.R. Salim, Fundamentals of mass transfer and kinetics for biosorption of oil and grease from agro-food industrial effluent by Serratia marcescens SA30, RSC Adv., 5 (2015) 104666–104673.
[49] A. Itodo, F. Abdulrahman, L. Hassan, S. Maigandi, H. Itodo, Intraparticle diffusion and intraparticulate diffusivities of herbicide on derived activated carbon, Researcherm, 2 (2010) 74–86.
[50] F.-C. Wu, R.-L. Tseng, R.-S. Juang, Initial behavior of intraparticle diffusion model used in the description of adsorption kinetics, Chem. Eng. J., 153 (2009) 1–8.
[51] A. Özcan, E.M. Öncü, A.S. Özcan, Adsorption of Acid Blue 193 from aqueous solutions onto DEDMA-sepiolite, J. Hazard. Mater., 129 (2006) 244–252.
[52] M. Kapur, M.K. Mondal, Mass transfer and related phenomena for Cr (VI) adsorption from aqueous solutions onto Mangifera indica sawdust, Chem. Eng. J., 218 (2013) 138–146.
[53] G. Walker, L. Hansen, J.-A. Hanna, S. Allen, Kinetics of a reactive dye adsorption onto dolomitic sorbents, Water Res., 37 (2003) 2081.